Critical coupling vortex with grating-induced high Q-factor optical Tamm states

RASHID G. BIKBAEV,[1,2,*] **DMITRII N. MAKSIMOV,**[1,2] **PAVEL S. PANKIN,**[1,2] **KUO-PING CHEN,**[3] **AND IVAN V. TIMOFEEV**[1,2]

[1]*Kirensky Institute of Physics, Federal Research Center KSC SB RAS, Krasnoyarsk 660036, Russia*
[2]*Siberian Federal University, Krasnoyarsk 660041, Russia*
[3]*Institute of Imaging and Biomedical Photonics, National Chiao Tung University, 71150 Tainan, Taiwan*
[*]*bikbaev@iph.krasn.ru*

Abstract: We investigate optical Tamm states supported by a dielectric grating placed on top of a distributed Bragg reflector. It is found that under certain conditions the Tamm state may become a bound state in the continuum. The bound state, in its turn, induces the effect of critical coupling with the reflectance amplitude reaching an exact zero. We demonstrate that the critical coupling point is located in the core of a vortex of the reflection amplitude gradient in the space of the wavelength and angle of incidence. The emergence of the vortex is explained by the coupled mode theory.

1. Introduction

The combination of plasmonic and photonic structures leads to hybrid systems which have been of great interest in the recent years. One example of such a hybrid system is a two-dimensional lattice of nanoparticles combined with a Fabry-Perot resonator [1,2]. The unique properties of such systems can be applied to narrowband absorbers [3], lasers [4], sensors [5] and photodetectors [6]. The hybrid systems are used to reduce losses in plasmonics [7] and for local amplification of the electromagnetic field [8]. Hybrid two-dimensional lattices not only act as structural elements but can also be used as mirrors for engineering localized states such as Tamm plasmon-polariton (TPP) [9–16]. The TPP is an optical analogue of the Tamm electronic states from solid state physics [17]. In contrast to conventional surface plasmon-polariton (SPP), the TPP can be both TM and TE polarized when their frequencies are above the light cone [18]. The TTPs usually possess larger absorption *Q*-factor than the SPPs. This is because of low material losses and larger resonant volume due to Bragg reflectors [19].

It was recently shown [20] that a TPP can be excited at the interface between binary Au nanodisk arrays and distributed Bragg reflector (DBR). In this case the coupling between the TPP and a localized lattice resonant mode results in dual Tamm states. The described structure can be used to measure the Zak phase. Thus, in [21] the Zak phase has been determined through the interface state. The propagation of the Tamm plasmons was investigated in [22] by depositing metallic stripes on top of a semiconductor Bragg mirror. It was shown that the TPPs are coupled to surface plasmons arising at the stripe edges. These plasmons form an interference pattern close to the bottom surface of the stripe resulting in a change of both the energy and loss rate for the TPP.

The disadvantage of the hybrid systems is material losses. Therefore, dielectric metasurfaces are increasingly used. For example in [23] the authors propose narrowband perfect absorbers with enormously high fabrication tolerance, that consist of a low-contrast grating and a finite DBR layer with an ultrathin absorbing medium (graphene). A planar array of optical band-pass filters composed of low loss dielectric metasurface layers sandwiched between two DBRs is reported in [24]. The surface states, known as optical Tamm states (OTS), can also be supported by all-dielectric structures [25–27]. By definition the OTS are surface states which exist on the

surface of a bulk material with the eigenfrequencies embedded into the material bandgap [28,29]. The OTS in all-dielectric structures are analogous to the conventional TPP and do not differ from the TPP in regard to their excitation or detection. The difference is in the terminology: an OTS in dielectric structures can not be called TPP due to the absence of plasmonic material. The OTS can be observed in both non-chiral [30,31] and chiral [32–34] structures.

Here we compare OTSs in all-dielectric and hybrid structures in the form of a DBR with a grating on its surface. We numerically demonstrate that the OTS in an all-dielectric structure has a larger quality factor than the TPP in the hybrid system.

Ultimately, in dielectric structures the OTS can obtain an infinite radiative quality factor, i.e. the OTS becomes optical bound state in the continuum (BIC) [35]. Such states supported by dielectric gratings have been previously reported both experimentally [36,37] and theoretically [38–41]. Here we focus on so-called *accidental* BICs [42] not protected by symmetry which occur as Bloch surface waves out of the Γ-point [43]. We demonstrate that such a Tamm BIC induces the effect of critical coupling (CC). We show that the CC corresponds to a phase singularity in the space of incidence angle and frequency, while the phase gradient forms a vortex with the CC point in the core. The phase singularities carry a topological charge [44] defined as the number of 2π windings of the phase along a closed contour around the CC point. Based on the temporal coupled mode theory [45] we derive a semi-analytic expression for the reflection amplitudes that matches well with our full-wave numerical simulations. The CC points are known to lead to very fast local variation of the phase of the reflection amplitude [46]. Here we find that such fast variation in the vicinity of the CC is unavoidable due to the phase singularity.

2. Model

Let us consider a DBR with a 2D array of silicon nanostripes [47] on top (Fig. 1(a)). The DBR unit cell is formed of two layers: silica dioxide (SiO_2) with thickness $d_a = 165$ nm and permittivity $\varepsilon_a = 2.1$, and zirconium dioxide (ZrO_2) with thickness $d_b = 135$ nm and permittivity $\varepsilon_b = 4.16$. The 2D structure with thickness h and width L has infinite length along y axis with period p. The multilayer structure can be fabricated by chemical vapor deposition, while the two-dimensional lattice of Si nanostripes can be patterned with e-beam lithography. The propagation direction and polarization of the incident plane wave are shown by the red and blue arrows, respectively. The optical properties of the structures have been calculated by commercial Finite-Difference Time-Domain (FDTD) package.
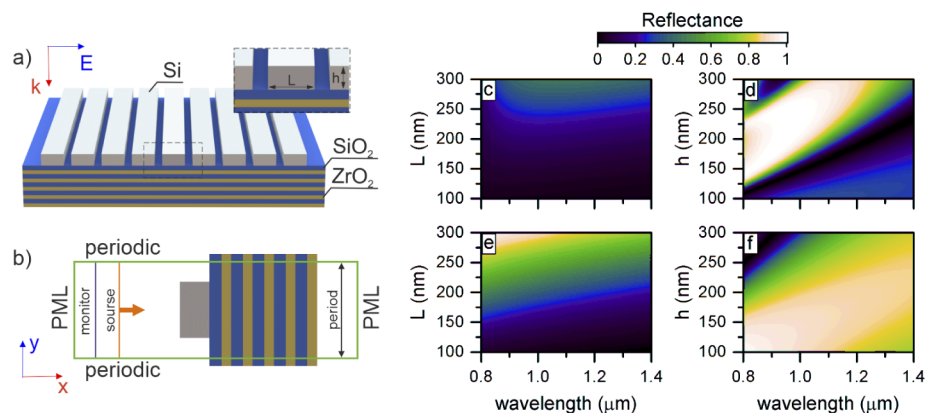
Fig. 1. (a) Schematic representation of the structure and (b) sketch view of the simulation box. Reflectance spectra of the 2D silicon (c,d) and gold (e,f) stripes array for different value of thickness L (c,e) ($h = 100$ nm) and h (d,f) ($L = 300$ nm). Period of the array $p = 400$ nm.

The simulation box is shown in Fig. 1(b). The PhC structure is illuminated from the top by a plane wave with its k in **E** vectors in the $x0y$ plane as shown in Fig. 1. The reflectance R is calculated at the top of the simulation box. Periodic boundary conditions are applied at the lateral boundaries of the simulation box, while perfectly matched layer (PML) boundary conditions were used on the remaining top and bottom interfaces.

3. Results

3.1. Reflection from bare 2D structure

A localized state, such as OTS, can be formed at the boundary of reflecting media. In our structure, reflection from a DBR is provided by the photonic band gap. If the number of layers is infinite the layered DBR forms an ideal Bragg reflector [43] which prohibits radiation losses. Reflection from the 2D structure can be controlled by varying the angle of incidence and lattice period, as well as the thickness and width of the nanostripes. First we calculated the reflectance spectra of the bare 2D structure without a DBR. The simulation results are shown in Figs. 1(c)-(f).

The calculations were carried out in two steps. In the initial step, we fixed the height of the stripes and varied their width. Thus, the width at which the most reflection from the structure is achieved was determined. In the next step, we varied the height of the stripe with fixed width. In this way we were able to determine the parameters of the structure at which the largest reflection from the structure can be achieved. The calculation results showed that the largest reflection is achieved in the range from 800 to 1200 nm for a structure with a stripes thickness $h = 250$ nm and a width of $L = 300$ nm (see Figs. 1(c) and (d)). We also calculated the reflectance spectra of a 2D array of gold stripes. The results are presented in the Figs. 1(e) and (f), which shows that the structure reflects in the entire range of wavelengths investigated, but the reflectance is not high, and reaches only 60-70%. We determined that the reflection reaches the maximum value for stripes with thickness $h = 150$ nm and width $L = 300$ nm.

3.2. OTS in an all-dielectric structure

We expect that conjugation of the grating with a DBR could lead to the formation of localized states, since the radiation to the lower half-space is suppressed by the band-gap whereas radiation into the upper half-space is reduced by the 2D structure acting as a mirror [43]. To verify this the reflectance spectra of the composite structures were calculated (see Fig. 2). Figure 2(a) shows that the DBR band gap in the range from 900 to 1100 nm overlaps with the reflection region of a 2D silicon stripes structure. In the area of their overlap, a narrow spectral line ($\lambda = 1060$ nm) is observed within the photonic band gap. This line corresponds to a state localised at the interface between DBR and 2D array of silicon stripes.
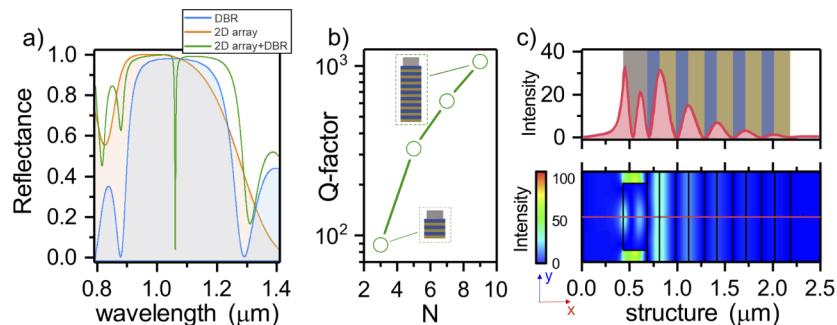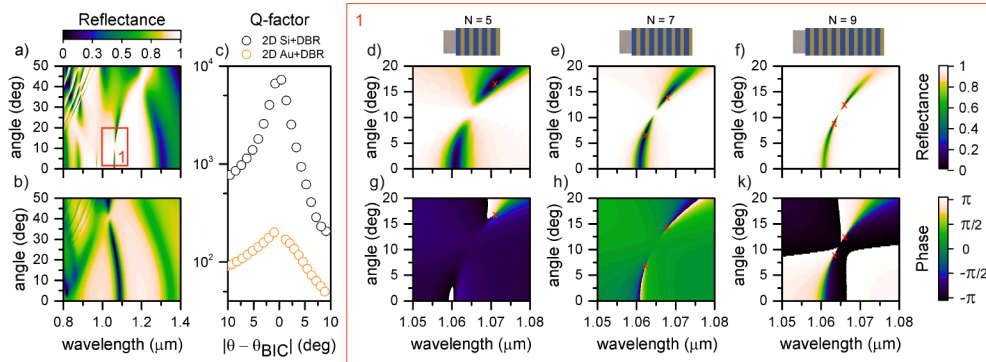

Fig. 2. (a) Reflectance spectra of the structure. (b) The Q-factor of the OTS depends on the number of DBR layers and (c) field distribution at the OTS wavelength.

It is important to note that the increase of the number of periods in the DBR leads to a significant increase in the Q-factor of the resonance (see Fig. 2(b)). Thus, when increasing N from 3 to 9, the Q-factor grows by more than an order of magnitude. This because the increase in the number of periods of the DBR leads to a decrease of the radiative decay rate in the lower half-space. When the DBR is infinite, the losses into the lower half-space are totally suppressed by the photonic band gap, whereas the losses to the upper half-space are suppressed by interference [43].

The distribution of the field intensity at the wavelength of the localized state is shown in the Fig. 2(c). On can see that the field is localized close to the interface between the two constituent subsystems and exponentially decreases in the photonic crystal and the 2D lattice. However, unlike conventional OTS, in our case the field is also localized on the front border of the 2D medium. The maximum intensity of the field is achieved not in the center of the stripe, but at its boundaries (see bottom subplot in Fig. 2(c)). This leads to enhancement of the field in the inter-stripe space.

The angular dependence of the reflectance spectra is shown in the Fig. 3. The figure shows that the spectra of the localized state for DBR bounded by 2D silicon or gold structure are cardinally different, see Figs. 3(a) and (b). The figure shows that the Q-factor of the localized state for Si structure is much larger than in the hybrid set-up. This difference is observed in the entire range of the angles of incidence, see Fig. 3(c). It should be noted that the difference is not only in the width of the resonance, but also in its shift with the increase of the angle of incidence. For gold stripes the localized state is shifted to the blue, same as for the conventional TPP [9,28,48], while for silicon stripes, we observe a red shift. It is worth mentioning that the red shift of TM-polarized localized state was recently predicted in [16]. Moreover, in both cases, we see the collapse of the resonant lines, with the only difference that for silicon stripe structure, this effect is observed at lower angles. Thus, the OTS becomes a non-radiating state, i.e. a BIC, at a specific incidence angle $\theta \approx 10.9°$. Such BICs are robust as they are topologically protected due to polarization singularities in the far field polarization patterns [49]. However, the exact nature of the interference mechanism leading an off-Γ BIC at a certain angle of incidence is currently only a subject of ongoing research. One promising approach is analyzing multipolar decomposition of the eigenmode within the elementary cell [50]. Such an analysis leads to an eigenfield with its node in the radiation pattern at the angle of the BIC.

Fig. 3. Reflectance spectra of the structure in case of (a) silicon and (b) gold stripes. (c) Q-factor of the structures near BIC points. (d,e,f) Reflectance spectra and (g,h,k) reflection phase of the DBR bounded by 2D silicon stripes for different number of DBR periods. Red crosses indicate CC points and phase singularities.

To look at the dielectric structure in more detail we calculated the reflection spectra of the structure and phase of the reflected wave in the region of the collapse of the resonance line. The calculation results are shown in Figs. 3(d)-(k). It can be seen from the reflection spectra that the increase of N leads to the contraction of the resonant lines in the BIC point. By a detailed examination of Figs. 3(d)-(k) one can observe critical coupling points, where the reflection coefficient is zero. For $N = 5$, see Fig. 3(g), only one critical coupling point is observed, while for $N = 7$ and $N = 9$, see Figs. 3(h) and (k) two critical coupling points are present. One can see that the two points approach one another with the increase of N. As the calculations have shown, even at $N = 9$, we do not see merging of the two CC points. Further increase of N up to infinity would allow us to achieve this effect if the material losses are neglected, but in this case we would meet difficulties both with simulations and experimental implementation. In Figs. 4(a) and (b) we plotted the absorptance spectrum for Si structure. One can see that absorptance reaches its maxima in the CC points, yet, even with $N = 9$ most of the radiation is transmitted due to the tunneling through the bandgap. Finally, it is worth to stress that the presence of material losses does not eliminate the effect of BIC which in the case of an infinitely thick DBR is an ideally non-radiating localized state. This state, however, has a finial life-time due to absorption. The Q-factor of such a state is only limited by material losses in the host structure. BICs in lossy structures have been recently analysed in [51] in application to enhanced absorption in the critical coupling point.
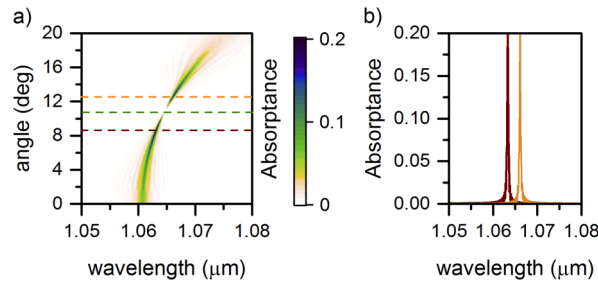
Fig. 4. (a) Absorptance spectra of the Si+DBR structure with $N = 9$ for different angles of incidence; and (b) absorptance spectra of the structure at CC and BIC angles (dotted line in figure a).

3.3. *Coupled mode theory*

The scattering spectrum in the vicinity of a localized state can be described in the framework of the temporal coupled mode theory [45]. According to the temporal coupled mode theory the reflection amplitude can be written as follows

$$r = e^{i2\eta} \left(-1 + \frac{2\gamma_1(\theta)}{i[\omega - \bar{\omega}(\theta)] + \gamma_1(\theta) + \gamma_2} \right), \tag{1}$$

where ω is the frequency of the incident wave, $\bar{\omega}$ - the resonant frequency, η - global phase, θ - the angle of incidence, γ_1 is the loss rate due to coupling to the upper lower half-space, and γ_2 is the loss rate due to both absorption and the bandgap tunneling. The latter two effects can be incorporated into a single constant since both can be regarded as non-dispersive. In the upper half-space though, the coupling is dependent on θ and cancelled by destructive interference only if $\theta = \theta_{\text{BIC}}$. By setting $r = 0$ one immediately arrives at the condition for the CC

$$\omega = \bar{\omega}(\theta_{\text{CC}}),$$
$$\gamma_2 = \gamma_1(\theta_{\text{CC}}). \tag{2}$$

Since we have two parameters to satisfy two equations the CCs are points in the plane of θ and ω. One can immediately see from Eq. (2) that in case of a true BIC with no absorption, $N = \infty$ and $\gamma_2 = 0$ the two CC points merge with the BIC. The dispersion of the entries of Eq. (1) are given by [52]

$$\bar{\omega} = \omega_0 - \alpha\theta^2 + O(\theta^4),$$
$$\gamma_1 = \beta(\theta^2 - \theta_{\mathrm{BIC}}^2)^2 + O\left[(\theta^2 - \theta_{\mathrm{BIC}}^2)^4\right],$$

(3)

where we took into account the symmetry of the leaky band about the Γ-point. Notice that $\gamma_1 = 0$ in the BIC point. Equation (3) contains two unknowns, α and β. The first, α, can be easily found by fitting to the Lorentzian center-frequency in Fig. 3(d). The second parameter, β, can be derived as

$$\beta = \frac{\gamma_2}{(\theta_{\mathrm{CC}}^2 - \theta_{\mathrm{BIC}}^2)^2},$$

(4)

$2\gamma_2$ being the half-width of the Lorentzian at the CC angle. Equation (1) predicts an exact zero of the reflection coefficients. The existence of an exact zero can be proven by the phase singularity with the phase of the reflection coefficient undetermined in the CC points. The phase singularity manifests itself in the vortical behaviour of the gradient of the phase, ϕ [44] of the reflection coefficient in space of θ and ω. The phase ϕ in Eq. (5) is implicitly defined via $r = |r|e^{i\phi}$. Although the phase is not uniquely defined due to 2π windings around the CC point, the gradient is a well-behaved function and, thus, can be derived analytically from Eq. (1), by using the following equation

$$\nabla\phi = \frac{r^*\nabla r - r\nabla r^*}{2i|r|^2}.$$

(5)

We spare the reader of the cumbersome equations resulting from Eq. (1) and Eq. (5). Notice, though, that since the global phase η is independent of both θ and λ it is absent from Eq. (5).
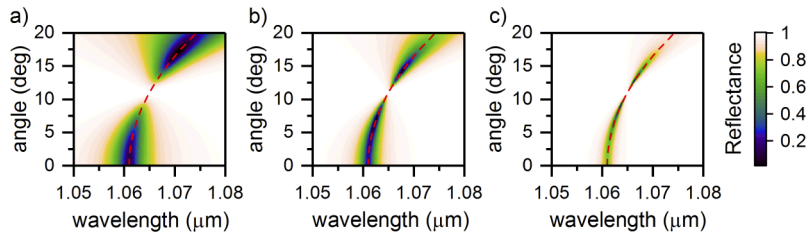
Fig. 5. Reflectance spectra of the DBR bounded by 2D silicon stripes for different number of DBR periods (a) $N = 5$, (b) $N = 7$, (c) $N = 9$ obtained by coupled mode theory. The red dotted line represent the direction curve of the OTS.
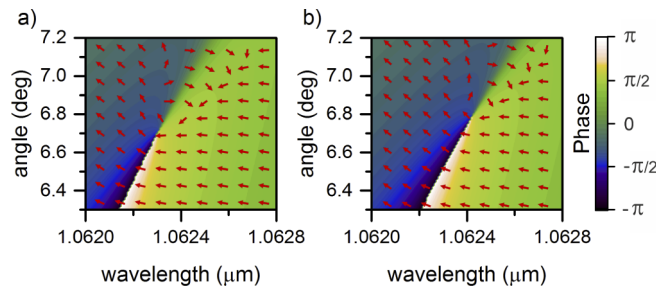
Fig. 6. Reflection phase of the DBR bounded by 2D lattice for N=7 obtained by (a) FDTD and (b) coupled mode theory. The red arrows represent the direction of the phase gradient.

In Fig. 5 we show the reflectance spectra of the systems with different numbers of DBR periods obtained with the use of the temporal coupled-mode theory. By comparing Fig. 5 against Figs. 3(d)-(f) one can see that Eq. (1) allowed us to reproduce the reflectance spectra of the system in a large range of incidence angles and frequencies. Finally, we compare the results obtained with Eq. (5) against the results of full-wave numerical simulations near the CC point. Figure 6 shows the phase of the wave reflected from the structure and the direction of the phase gradient near one of the critical coupling points represented in Fig. 5(b). One can see that the results are in good agreement and the critical coupling vortex is observed in both cases.

4. Conclusion

In summary, we showed that optical Tamm state in all-dielectric system possess a *Q*-factor larger than in hybrid plasmonic dielectric systems. This, in turn, makes it possible to engineer a structure supporting an optical Tamm state with the radiation loss rate much smaller than the loss rate due to the light absorption in the structure material. We demonstrated that the presence of such states lead to the critical coupling effect. The critical coupling is associated with a phase singularity of the reflection coefficient in the space of wavelength and angle of incidence of the impinging plane wave. The scattering spectrum is explained by a single resonance coupled mode approach. The resulting equation is found to correctly account of the topological property of the critical coupling vortex. We speculate that the results presented open novel opportunities in engineering critical coupling, whereas the phase singularity yields unlimited sensitivity to variation of the system's parameters paving a way to sensing applications. We believe that the proposed design scheme can be further improved by applying perfect reflectors based on periodic arrays of rods with cylindrical cross-section [53,54]. Such perfectly reflecting mirrors can replace the bar grating analysed in the present paper.

Disclosures. The authors declare no conflicts of interest.

References

1. R. Ameling and H. Giessen, "Microcavity plasmonics: strong coupling of photonic cavities and plasmons," Laser Photonics Rev. **7**(2), 141–169 (2013).
2. V. Gerasimov, A. Ershov, R. Bikbaev, I. Rasskazov, I. Timofeev, S. Polyutov, and S. Karpov, "Engineering mode hybridization in regular arrays of plasmonic nanoparticles embedded in 1D photonic crystal," J. Quant. Spectrosc. Radiat. Transfer **224**, 303–308 (2019).
3. D. Chanda, K. Shigeta, T. Truong, E. Lui, A. Mihi, M. Schulmerich, P. V. Braun, R. Bhargava, and J. A. Rogers, "Coupling of plasmonic and optical cavity modes in quasi-three-dimensional plasmonic crystals," Nat. Commun. **2**(1), 477–479 (2011).
4. W. Zhou, M. Dridi, J. Y. Suh, C. H. Kim, D. T. Co, M. R. Wasielewski, G. C. Schatz, and T. W. Odom, "Lasing action in strongly coupled plasmonic nanocavity arrays," Nat. Nanotechnol. **8**(7), 506–511 (2013).
5. J. Chen, Q. Zhang, C. Peng, C. Tang, X. Shen, L. Deng, and G.-S. Park, "Optical Cavity-Enhanced Localized Surface Plasmon Resonance for High-Quality Sensing," IEEE Photonics Technol. Lett. **30**(8), 728–731 (2018).
6. R. J. Thompson, T. Siday, S. Glass, T. S. Luk, J. L. Reno, I. Brener, and O. Mitrofanov, "Optically thin hybrid cavity for terahertz photo-conductive detectors," Appl. Phys. Lett. **110**(4), 041105 (2017).
7. R. Kamakura, S. Murai, S. Ishii, T. Nagao, K. Fujita, and K. Tanaka, "Plasmonic–Photonic Hybrid Modes Excited on a Titanium Nitride Nanoparticle Array in the Visible Region," ACS Photonics **4**(4), 815–822 (2017).
8. S. Alrasheed and E. Di Fabrizio, "Effect of Surface Plasmon Coupling to Optical Cavity Modes on the Field Enhancement and Spectral Response of Dimer-Based sensors," Sci. Rep. **7**(1), 10524 (2017).
9. M. Kaliteevski, I. Iorsh, S. Brand, R. A. Abram, J. M. Chamberlain, A. V. Kavokin, and I. A. Shelykh, "Tamm plasmon-polaritons: Possible electromagnetic states at the interface of a metal and a dielectric Bragg mirror," Phys. Rev. B **76**(16), 165415 (2007).
10. Z.-Y. Yang, S. Ishii, T. Yokoyama, T. D. Dao, M.-G. Sun, P. S. Pankin, I. Timofeev, T. Nagao, and K.-P. Chen, "Narrowband Wavelength Selective Thermal Emitters by Confined Tamm Plasmon Polaritons," ACS Photonics **4**(9), 2212–2219 (2017).
11. H. Lu, X. Gan, B. Jia, D. Mao, and J. Zhao, "Tunable high-efficiency light absorption of monolayer graphene via Tamm plasmon polaritons," Opt. Lett. **41**(20), 4743–4746 (2016).

12. H. Lu, Y. Li, Z. Yue, D. Mao, and J. Zhao, "Topological insulator based Tamm plasmon polaritons," APL Photonics **4**(4), 040801 (2019).

13. R. Bikbaev, S. Vetrov, and I. Timofeev, "Epsilon-Near-Zero Absorber by Tamm Plasmon Polariton," Photonics **6**(1), 28 (2019).

14. A. M. Vyunishev, R. G. Bikbaev, S. E. Svyakhovskiy, I. V. Timofeev, P. S. Pankin, S. A. Evlashin, S. Y. Vetrov, S. A. Myslivets, and V. G. Arkhipin, "Broadband Tamm plasmon polariton," J. Opt. Soc. Am. B **36**(8), 2299–2305 (2019).

15. E. I. Girshova, A. P. Mikitchuk, A. V. Belonovski, K. M. Morozov, K. A. Ivanov, G. Pozina, K. V. Kozadaev, A. Y. Egorov, and M. A. Kaliteevski, "Proposal for a photoacoustic ultrasonic generator based on Tamm plasmon structures," Opt. Express **28**(18), 26161–26169 (2020).

16. J. Wu, F. Wu, C. Xue, Z. Guo, H. Jiang, Y. Sun, Y. Li, and H. Chen, "Wide-angle ultrasensitive biosensors based on edge states in heterostructures containing hyperbolic metamaterials," Opt. Express **27**(17), 24835–24846 (2019).

17. I. E. Tamm, "Tamm_t1_1975ru.pdf," Phys. Z. Sowjetunion **1**, 733 (1932).

18. A. P. Vinogradov, A. V. Dorofeenko, A. M. Merzlikin, and A. a. Lisyansky, "Surface states in photonic crystals," Phys.-Usp. **53**(3), 243–256 (2010).

19. C. Symonds, S. Azzini, G. Lheureux, A. Piednoir, J. M. Benoit, A. Lemaitre, P. Senellart, and J. Bellessa, "High quality factor confined Tamm modes," Sci. Rep. **7**(1), 3859 (2017).

20. L. Wang and Y. Jiang, "Confined dual hybrid states through coupling Tamm plasmon and localized lattice resonance," Proc. SPIE **10824** 108240F (2018).

21. Q. Wang, M. Xiao, H. Liu, S. Zhu, and C. T. Chan, "Measurement of the zak phase of photonic bands through the interface states of a metasurface/photonic crystal," Phys. Rev. B **93**(4), 041415 (2016).

22. I. Y. Chestnov, E. S. Sedov, S. V. Kutrovskaya, A. O. Kucherik, S. M. Arakelian, and A. V. Kavokin, "One-dimensional tamm plasmons: Spatial confinement, propagation, and polarization properties," Phys. Rev. B **96**(24), 245309 (2017).

23. S. Lee, H. Heo, and S. Kim, "High fabrication-tolerant narrowband perfect graphene absorber based on guided-mode resonance in distributed bragg reflector," Sci. Rep. **9**(1), 4294 (2019).

24. Y. Horie, A. Arbabi, E. Arbabi, S. M. Kamali, and A. Faraon, "Wide bandwidth and high resolution planar filter array based on DBR-metasurface-DBR structures," Opt. Express **24**(11), 11677 (2016).

25. L. Jiang, J. Tang, Q. Wang, Y. Wu, Z. Zheng, Y. Xiang, and X. Dai, "Manipulating optical Tamm state in the terahertz frequency range with graphene," Chin. Opt. Lett. **17**(2), 020008 (2019).

26. W. L. Zhang, F. Wang, Y. J. Rao, and Y. Jiang, "Novel sensing concept based on optical Tamm plasmon," Opt. Express **22**(12), 14524–14529 (2014).

27. D. Dong, Y. Liu, and Y. Fu, "Enhancing the Faraday rotation of monolayer black phosphorus by the optical Tamm state at the photonic crystal interface," Appl. Opt. **59**(30), 9607–9613 (2020).

28. A. V. Kavokin, I. A. Shelykh, and G. Malpuech, "Lossless interface modes at the boundary between two periodic dielectric structures," Phys. Rev. B **72**(23), 233102 (2005).

29. A. P. Vinogradov, A. V. Dorofeenko, S. G. Erokhin, M. Inoue, A. A. Lisyansky, A. M. Merzlikin, and A. B. Granovsky, "Surface state peculiarities in one-dimensional photonic crystal interfaces," Phys. Rev. B **74**(4), 045128 (2006).

30. Y. Yang and Y. Pan, "Engineering zero modes, Fano resonance, and Tamm surface states in the waveguide-array realization of the modified Su-Schrieffer-Heeger model," Opt. Express **27**(23), 32900–32911 (2019).

31. Y. Fei, Y. Liu, D. Dong, K. Gao, S. Ren, and Y. Fan, "Multiple adjustable optical Tamm states in one-dimensional photonic quasicrystals with predesigned bandgaps," Opt. Express **26**(26), 34872–34879 (2018).

32. I. Timofeev and S. Y. Vetrov, "Chiral optical Tamm states at the boundary of the medium with helical symmetry of the dielectric tensor," JETP Lett. **104**(6), 380–383 (2016).

33. N. V. Rudakova, I. V. Timofeev, R. G. Bikbaev, M. V. Pyatnov, S. Y. Vetrov, and W. Lee, "Chiral Optical Tamm States at the Interface between an All-Dielectric Polarization-Preserving Anisotropic Mirror and a Cholesteric Liquid Crystal," Crystals **9**(10), 502 (2019).

34. A. Y. Avdeeva, S. Y. Vetrov, R. G. Bikbaev, M. V. Pyatnov, N. V. Rudakova, and I. V. Timofeev, "Chiral Optical Tamm States at the Interface between a Dye-Doped Cholesteric Liquid Crystal and an Anisotropic Mirror," Materials **13**(15), 3255 (2020).

35. C. W. Hsu, B. Zhen, A. D. Stone, J. D. Joannopoulos, and M. Soljačić, "Bound states in the continuum," Nat. Rev. Mater. **1**(9), 16048 (2016).

36. Z. F. Sadrieva, I. S. Sinev, K. L. Koshelev, A. Samusev, I. V. Iorsh, O. Takayama, R. Malureanu, A. A. Bogdanov, and A. V. Lavrinenko, "Transition from optical bound states in the continuum to leaky resonances: Role of substrate and roughness," ACS Photonics **4**(4), 723–727 (2017).

37. H. M. Doeleman, F. Monticone, W. den Hollander, A. Alù, and A. F. Koenderink, "Experimental observation of a polarization vortex at an optical bound state in the continuum," Nat. Photonics **12**(7), 397–401 (2018).

38. Y. Wang, J. Song, L. Dong, and M. Lu, "Optical bound states in slotted high-contrast gratings," J. Opt. Soc. Am. B **33**(12), 2472–2479 (2016).

39. E. N. Bulgakov, D. N. Maksimov, P. N. Semina, and S. A. Skorobogatov, "Propagating bound states in the continuum in dielectric gratings," J. Opt. Soc. Am. B **35**(6), 1218–1222 (2018).

40. E. N. Bulgakov and D. N. Maksimov, "Avoided crossings and bound states in the continuum in low-contrast dielectric gratings," Phys. Rev. A **98**(5), 053840 (2018).

41. F. Wu, J. Wu, Z. Guo, H. Jiang, Y. Sun, Y. Li, J. Ren, and H. Chen, "Giant enhancement of the goos-hänchen shift assisted by quasibound states in the continuum," Phys. Rev. Appl. **12**(1), 014028 (2019).

42. C. W. Hsu, B. Zhen, J. Lee, S.-L. Chua, S. G. Johnson, J. D. Joannopoulos, and M. Soljačić, "Observation of trapped light within the radiation continuum," Nature **499**(7457), 188–191 (2013).

43. C. W. Hsu, B. Zhen, S.-L. Chua, S. G. Johnson, J. D. Joannopoulos, and M. Soljačić, "Bloch surface eigenstates within the radiation continuum," Light: Sci. Appl. **2**(7), e84 (2013).

44. K. Y. Bliokh, M. A. Alonso, and M. R. Dennis, "Geometric phases in 2d and 3d polarized fields: geometrical, dynamical, and topological aspects," Rep. Prog. Phys. **82**(12), 122401 (2019).

45. S. Fan, W. Suh, and J. D. Joannopoulos, "Temporal coupled-mode theory for the fano resonance in optical resonators," J. Opt. Soc. Am. A **20**(3), 569 (2003).

46. Y. Tsurimaki, J. K. Tong, V. N. Boriskin, A. Semenov, M. I. Ayzatsky, Y. P. Machekhin, G. Chen, and S. V. Boriskina, "Topological engineering of interfacial optical tamm states for highly sensitive near-singular-phase optical detection," ACS Photonics **5**(3), 929–938 (2018).

47. D. F. Edwards, "Silicon (Si)," in *Handbook of Optical Constants of Solids*, (Elsevier, 1997), pp. 547–569.

48. S. Nú nez-Sánchez, M. Lopez-Garcia, M. M. Murshidy, A. G. Abdel-Hady, M. Serry, A. M. Adawi, J. G. Rarity, R. Oulton, and W. L. Barnes, "Excitonic optical tamm states: A step toward a full molecular-dielectric photonic integration," ACS Photonics **3**(5), 743–748 (2016).

49. B. Zhen, C. W. Hsu, L. Lu, A. D. Stone, and M. Soljačić, "Topological nature of optical bound states in the continuum," Phys. Rev. Lett. **113**(25), 257401 (2014).

50. Z. Sadrieva, K. Frizyuk, M. Petrov, Y. Kivshar, and A. Bogdanov, "Multipolar origin of bound states in the continuum," Phys. Rev. B **100**(11), 115303 (2019).

51. X. Wang, J. Duan, W. Chen, C. Zhou, T. Liu, and S. Xiao, "Controlling light absorption of graphene at critical coupling through magnetic dipole quasi-bound states in the continuum resonance," Phys. Rev. B **102**(15), 155432 (2020).

52. E. N. Bulgakov and D. N. Maksimov, "Topological bound states in the continuum in arrays of dielectric spheres," Phys. Rev. Lett. **118**(26), 267401 (2017).

53. W. Liu, "Generalized magnetic mirrors," Phys. Rev. Lett. **119**(12), 123902 (2017).

54. W. Tong, J. Luo, Z. Sun, and Y. Lai, "Perfect absorbers based on dielectric optical mirrors and ultrathin absorptive films," Appl. Phys. Express **13**(3), 032001 (2020).